Available online at www.sciencedirect.com
SCIENCE DIRECT
Catalysis Today 105 (2005) 516–528
CATALYSIS TODAY
www.elsevier.com/locate/cattod

# Optimization of anodic oxidation and Cu–Cr oxide catalyst preparation on structured aluminum plates processed by electro discharge machining

I.Z. Ismagilov [a,b], R.P. Ekatpure [a], L.T. Tsykoza [b], E.V. Matus [b], E.V. Rebrov [a], M.H.J.M. de Croon [a], M.A. Kerzhentsev [b], J.C. Schouten [a,*]

[a] *Laboratory of Chemical Reactor Engineering, Eindhoven University of Technology, P.O. Box 513, 5600 MB Eindhoven, The Netherlands*
[b] *Laboratory of Environmental Catalysis, Boreskov Institute of Catalysis SB RAS, Prospekt Akademika Lavrentieva, 5, Novosibirsk 630090, Russia*

**Abstract**

This paper describes the optimization of three processes applied in fabrication of a microstructured reactor for complete oxidation of volatile organic compounds. The first process involves the optimization of the electro discharge machining (EDM) method to produce a set of microchannels with a high length to diameter ratio of 100, with a standard deviation from the average diameter below 0.2%, and with a surface roughness not higher than 2.0 μm. To satisfy these criteria, fabrication of microchannels must be carried out with two machining passes in the Al51st alloy. Then, the effect of several parameters on the anodization current efficiency with respect to oxide formation was studied. The best process conditions to get a 30 μm porous alumina layer in a 0.4 M oxalic acid electrolyte, were found to be a temperature of 1 °C, an anodic current density of 5 mA/cm$^2$, and 23 h oxidation time. At last, the resulting coatings were impregnated with an aqueous solution of copper dichromate followed by drying and calcination at 450 °C to produce active catalysts. The effect of a copper dichromate concentration, number of impregnation cycles (1 or 2), and different after-treatments on catalytic activity and stability in complete oxidation of n-butane were studied. The catalytic activity of the obtained coatings is superior to that of alumina supported pelletized catalysts even at much lower loadings of active metals.


*Keywords:* Microstructured reactor; Electro discharge machining; Anodic oxidation; Copper chromite; Catalytic combustion; VOC

## 1. Introduction

In general, a high and uniform accessibility of catalytic sites is of great importance to get a high activity and a high selectivity in any chemical process. The objective of the present work is to obtain a uniform accessibility of a particular catalyst that is distributed over a large volume in a microstructured reactor. To reach this goal, it is important to create a uniform reactant flow distribution across the microchannels in this reactor as well as to obtain a uniform pore size distribution of the catalyst support material. Furthermore, it is relevant to develop the proper structure of the catalyst and its support.

A non-uniformity in the diameter of microchannels, created at different stages of microrector fabrication, can disturb considerably the residence time distribution, thereby decreasing the reactor performance. One of the goals of this study is to examine the effect of different treatments on dimensional quality of the geometry during electro discharge machining (EDM) and anodic oxidation. EDM is a machining method in which a voltage is applied through a dielectric medium between the tool electrode and a workpiece, using electro-discharge generated when electrode and workpiece are positioned close to each other. Many researchers have used EDM to obtain microchannels in

* Corresponding author. Tel.: +31 40 247 2850; fax: +31 40 244 6653.
*E-mail address:* j.c.schouten@tue.nl (J.C. Schouten).

0920-5861/$ – see front matter © 2005 Elsevier B.V. All rights reserved.
doi:10.1016/j.cattod.2005.06.053

different metals. However, data relating to differences between different methods of EDM remain rare. Thus, we have focused in this study on the dimensional accuracy of methods of one, two and three machining passes applied to two different aluminum alloys. Aluminum based alloys were chosen as a substrate material because of their high thermal conductivity and high corrosion stability, as well as the possibility to form coatings of aluminum oxide. These coatings were reported to be effective catalyst supports [1–4]. They can be grown to a thickness of tens to hundreds of micrometers [2,3,5,6] and exhibit specific surface areas of 10–40 $m^2/g$ [2–4].

Microreactors are typically built up from several dozens up to several thousands of individual channels. Therefore, the anodic oxidation procedure is repeated by application of a number of oxidation runs until a desired number of substrate plates is obtained. In a classical procedure, the aluminum substrate is placed in the solution of a weak organic acid, which is used as electrolyte. In an electrolysis cell, the aluminum cathodes are usually applied. However, uniform coating properties, such as layer thickness and pore structure, are difficult to obtain in a subsequent set of oxidation runs, because the properties of the electrolyte are changing in the course of the electrolysis process, due to dissolution of alloying elements. Refreshing the electrolyte after each oxidation run would lead to a large amount of waste, which is not attractive from a practical point of view. Decreasing the volume of the electrolysis cell creates substantial problems in temperature control, due to heat evolution in the process. Recently, a method for scale-up of anodic oxidation was proposed. The anode, carrying ten aluminum plates, was slowly rotated in the electrolyte. The plates were thus cycled between the top and the bottom of the vessel and the materials were treated under the same conditions despite the temperature gradients present [7]. In our study, we propose a different concept for scale-up of the oxidation procedure, in which the electrolyte is circulating vertically in a vessel with a fixed anode, and a heat-exchanger is incorporated to remove the heat effectively. It will be demonstrated that such design allows to oxidize a large number of aluminum substrates under near isothermal conditions.

The microreactors to be developed from this study are intended for kinetic studies and optimization of the catalytic combustion of volatile organic compounds. In particular, we wish to study combustion of unsymmetrical dimethylhydrazine; a component of rocket fuel. Alumina supported copper chromite ($CuCr_2O_4$) has been selected as a catalyst because this is one of the most active and stable catalysts for complete oxidation of nitrogen containing organic compounds [8]. The direct formation of copper chromite from corresponding oxides typically proceeds above 500 °C [9]. An alumina supported copper chromite catalyst was prepared by impregnation with a copper dichromate solution followed by calcinations in air at 600 °C [10]. However, copper chromite can be formed under milder conditions (425–540 °C) upon decomposition of copper chromate ($CuCrO_4$) and copper dichromate ($Cu_2Cr_2O_7$), [11,12]. In this study, an attempt was made to obtain copper chromite coatings in the temperature range considerably below the melting point of the aluminum substrate in order to avoid its thermal deformation. The experimental procedures of catalyst preparation were studied and optimized to provide the most active and uniform catalytic coatings. The performance of catalytic coatings was studied in butane oxidation, which was chosen as a model reaction.

## 2. Experimental

### 2.1. EDM micromachining

Two types of aluminum were used: A199.5 (1050A series) and A151st (AlMgSi1 alloy, 6082 series, alloying elements Si: 1.0 wt.%, Mg: 0.9 wt.%, Cr: 0.15 wt.%, Zn: 0.1 wt.%, Mn: 0.7 wt.%, Cu: 0.1 wt.%). Microchannel fabrication tests with one machining pass were conducted using a low sparking energy by applying 80 V voltage, and a maximum current of 8 A with 1.0 μs ON and OFF time pulse durations. When a method with two machining passes is applied, a different generator code is used in the second pass: a voltage of 120 V, and a maximum current of 8 A with 0.2 μs ON and OFF time pulse durations. A copper electrode with a diameter of 250 μm coated with a zinc layer of ca. 1 μm (SW25X) was used. The plate was always connected to the positive polarity and the electrode to the negative polarity. Demineralized water (15 μS) was used as a dielectric medium. Machined microfeatures were examined using an optical microscope and a scanning electron microscope (SEM). The method with one machining pass was applied to fabricate a set of plates for optimization of anodic oxidation. The plates had a thickness of 430 μm. In each plate, 45 semi-cylindrical microchannels with a diameter of 388 μm and a distance of 500 μm between their centerlines were produced.

### 2.2. Anodic oxidation

In anodic oxidation experiments, the Al51st alloy was used. Two geometries of Al51st plates are studied. Flat plates of 35 mm × 20 mm with a thickness of 1 mm were oxidized to optimize the catalyst deposition techniques (A-plates). Also microstructured plates of 40 mm × 26.6 mm with a thickness of 430 μm, produced as described in Section 2.1, were oxidized to study the changes in geometry during oxidation (M-plates). The plates were first degreased in acetone at room temperature followed by boiling in xylene for 1 h. After that, the plates were dried at 300 °C in air for 1 h, cooled down and weighed. Then, the plates were immersed into a 1.0 M NaOH solution at 50 °C for 15 s. Afterwards, the plates were washed twice with distilled water and fixed in a holder in a 1.1 L electrolysis vessel. Two

platinum foils of 40 mm × 50 mm positioned at a distance of 10 cm from both sides of the aluminum plate were used as cathodes. A 25 μm alumina layer was produced on A-plates under current control conditions with an anodic current density of 15 mA/cm$^2$, in an aqueous 1.1 M oxalic acid solution at 7.0 °C. The electrolyte was continuously stirred by a magnetic stirrer. The apparent density of alumina was estimated to be 2.0 g/cm$^3$ based on a volume of the alumina layer of 0.0407 cm$^3$. The weight change due to oxygen incorporation of 0.0390 g corresponds to formation of 0.083 g of alumina. The metal losses due to aluminum dissolution in the electrolyte solution were negligible during oxidation of A-plates. The mass of aluminum incorporated in the alumina layer is equal to the mass decrease of aluminum. The mass of aluminum in the alumina layer was calculated based on its stoichiometry, apparent density and volume. The mass of aluminum was calculated based on a density of 2.7 cm$^3$/g and a thickness of the metal layer measured at a cross-section of the plate before and after oxidation. The latter was taken from SEM images. The porosity of the alumina layer was estimated to be 20%, the mean pore diameter was 40 nm, and the BET surface area was in the range 10–40 m$^2$/g.

Oxidation time and anodic current density were optimized with M-plates in a 0.4 M oxalic acid solution at 1.0 °C. A 10–20 μm layer of acrylic coating STAR12E (from Chemtronics®) was deposited to protect the flat side of M-plates from oxidation. After the oxidation process, this coating was removed by soaking in a high purity universal acrylic thinner solution UAT05L (from Electrolube®) at 50 °C. After the electrolysis, the plates were washed twice with distilled water, dried in air at 110 °C for 1 h, cooled and weighed.

A 20 L electrolysis vessel was constructed to produce a large set of anodized plates from the same electrolyte composition (Fig. 1). In this design, two aluminum (Al 99.5) cylindrical cathode foils were placed at a distance of 20 cm from each other. The length of the internal cathode was 75 cm and that of the external cathode was 200 cm. The height of both cathodes was 8 cm. Several geometrical parameters of the impeller were optimized to provide an effective electrolyte circulation from and to the impeller via twelve half-circle openings with a diameter of 3 cm made in the top and bottom parts of the internal cathode. Up to twelve aluminum substrates can be positioned on an aluminum ring between the cathode foils. The aluminum ring was connected to an anode. A PTFE line (carbon filled Polytetrafluorethylen, heat conductivity of 1 W m$^{-1}$ K$^{-1}$, i.d. = 8 mm, o.d. = 10 mm) for the coolant was fixed at the bottom part of the vessel. The temperature of the electrolyte in the vessel was controlled by a West 6100+ regulator by changing the temperature of coolant in the range from −15 to −5 °C depending on the heat evolved in the process.

### 2.3. Cu–Cr oxide catalyst deposition

Anodized Al51st plates were degreased with acetone and calcined at 300 °C. The catalysts were prepared by impregnation of the anodic alumina layer by an aqueous solution of copper dichromate, followed by drying under an IR lamp for 1 h and calcination at 450 °C for 4 h. The following conditions of catalyst preparation were varied: concentration of copper dichromate solution (250 or 500 mg/ml), duration of impregnation (0.1–1 h), number of impregnation cycles (1 or 2), mode of removal of excess impregnating solution (washing or wiping). The samples are

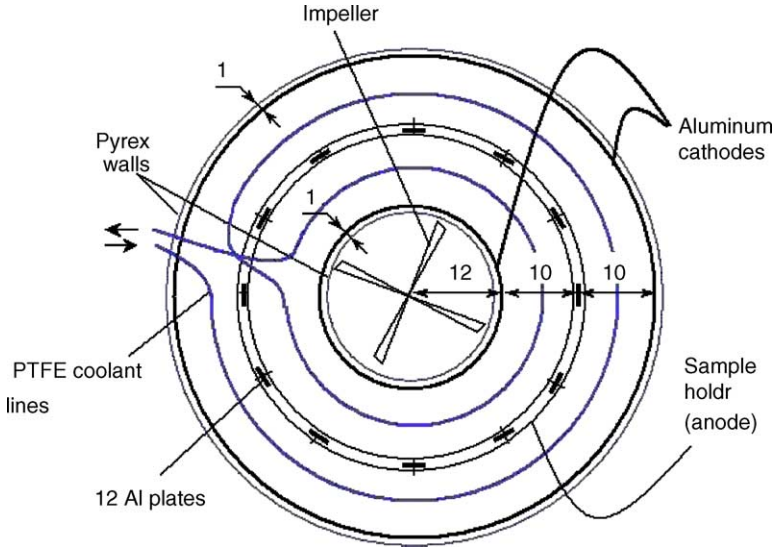


Fig. 1. Schematic view of a 20 l electrolysis vessel. Two aluminum cathode foils of 75 cm × 8 cm and 201 cm × 8 cm were placed at a distance of 20 cm from each other. Twelve half-circle openings with a diameter of 3 cm were made in the top and bottom parts of the internal cathode. A radial impeller was used with a diameter of 125 mm, with four blades,which were fixed to the axis at a distance of 40 mm from the bottom. The blade angle is 30°, and the blade height is 25 mm. The impeller speed was fixed at 160 rpm. Twelve aluminum substrates were positioned on an aluminum ring between the cathode foils. A PTFE line (i.d. = 8 mm, e.d. = 10 mm) for the coolant was fixed at the bottom part of the vessel. All sizes are given in millimetres.

referred to according to their loading with the active component and a number of impregnation cycles. Index ''A'' in the sample name stands for the flat Al plates, index ''M'' denotes the microstructured plates. Number in brackets corresponds to the $CuCr_2O_4$ loading and the Roman number stands for a number of impregnation cycles.

The reference samples of 26 wt.% $CuCr_2O_4/\gamma$-$Al_2O_3$ catalyst were prepared by incipient wetness impregnation of spherical γ-alumina granules (1.0–1.6 mm, the BET surface area is 193 $m^2/g$) with an aqueous solution of copper dichromate for 15 min. This was followed by drying under the IR lamp for 1 h and calcination in air at 400, 500 or 700 °C for 4 h to study the effect of the calcination temperature on the phase composition of copper-chromium oxide catalysts. These samples are referred as P(26)-400, P(26)-500, and P(26)-700 hereafter. The BET surface area of samples P(26)-500 and P(26)-700 is 129 and 106 $m^2/g$, respectively.

### 2.4. Catalyst characterization

The chemical composition of the samples was determined by inductively coupled plasma atomic emission spectroscopy (ICP-AES) after total dissolution of the sample in hydrochloric acid. The XRD studies were performed in a HZG-4 diffractometer using Cu Kα radiation in the $2\theta$ range of 10–70° with a sweep rate of 1° $2\theta$/min. X-ray microprobe analysis was performed on a MAP-3 microanalyzer with a probe diameter of ∼1 μm at the working voltage 25 kV and a current of 30–40 nA; Al Kα, Cu Kα and Cr Kα were the analytical lines. Fragments of 5 mm × 5 mm were fixed by epoxy resin in a holder. Textural characteristics of the samples were studied by nitrogen adsorption using an ASAP-2400 instrument. Diffuse reflectance spectra (DRS) were recorded by a spectrophotometer ''Shimadzu'' UV-2501 PC in the range of 11,000–54,000 $cm^{-1}$. X-ray photoelectron spectra were recorded using a spectrometer VG ESCALAB HP with Al Kα radiation. The carbon 1 s signal at 284.8 eV was used as a reference to calibrate the binding energy scale. The catalytic activity of the combustion catalysts was studied in the model reaction of butane oxidation in a flow setup with a tubular quartz reactor (i.d. of 13 mm) in the temperature range of 200–450 °C. The temperature was measured by a thermocouple placed downstream of the catalyst (granules or stack of plates). The original A or M-plates were cut for smaller fragments (5 mm × 20 mm). These fragments were loaded in the reactor at the distance of ∼0.5 mm from each other. The composition of the initial reaction mixture was 0.2 vol.% butane in air. The flow rate was adjusted to fix the same space velocity of 120,000 $h^{-1}$ with respect to the alumina volume. Butane, $O_2$, CO, $CO_2$, and $CH_4$ concentrations were analyzed using a ''Kristal-2000M'' GC equipped with FID and TCD detectors. A HayeSep S column (3 mm × 2 m) was used for butane separation and an activated carbon SKT column (3 mm × 2 m) was used for $CO_2$ separation from the gas mixture. Both columns were maintained at 165 °C. A molecular sieve NaX column (3 mm × 2 m) maintained at 20 °C was used for $O_2$, CO and $CH_4$ analysis. Neither carbon monoxide nor methane was found in the reaction products. The carbon balance was 95–105%. In some experiments, water was separated and analyzed using a Porapaq T column (3 mm × 2 m) maintained at 150 °C. The catalyst activity was characterized by the temperature dependence of the butane conversion to products of total oxidation ($CO_2$, $H_2O$).

## 3. Results and discussion

### 3.1. Fabrication of microchannels

We have chosen Al99.5 material for micromachining based on our previous experience to produce microreactors in aluminum [13–16]. However, in case of relatively long 40 mm plates, the results were quite different comparing with those for the 6.5 mm plates applied in [15] and [16]. The examination of microchannels obtained in this study and those in reference [15] revealed that the length of the workpiece has a large impact on material removal characteristics and results in different reproducibility even when the same material was used. In case of 40 mm long microchannels, application of the EDM method with one machining pass gave a relatively large standard deviation (S.D.) of the channel diameter (and the channel to channel distance) from the average values (S.D. = 1.4%), which would make the assembling of the microreactor impossible.

It is well known that Al51st material due to proper combination of alloying components, can be electro discharge machined in a more reproducible way. Indeed, the application of the same method gave a narrow channel diameter distribution of less than 0.34%. However, due to the different evaporation rate of aluminum and alloying components, a rough surface was obtained ($R_a$ = 4.0 μm). In attempt to reduce the surface roughness, the method with two machining passes was applied. In this method, the time interval between the sparks was decreased during the second machining pass. This allowed to obtain an $R_a$ value of 2.0 μm with further improvement of the channel diameter distribution (S.D. = 0.18%). Application of three machining passes deteriorated considerably the S.D. value, which was close to that of the Al99.5 material (S.D. = 1.2%). For the proper assembling of the reactor, a method with two machining passes had to be applied.

### 3.2. Anodic oxidation

Several studies have shown that anodization processes carried out at room and higher temperatures dramatically decrease the oxide formation current efficiency, leading to severe aluminum dissolution [3,17,18]. Therefore, in this study we decided to carry out the process just above the freezing point of the electrolyte. Aqueous oxalic acid

solutions become saturated above 0.6 M at 0 °C [19]. In our experiments, the oxalic acid concentration was fixed at 0.4 M. No substantial difference was observed in the oxidation behavior of the Al51st alloy machined with a method with one machining pass or with two machining passes. Therefore, the Al51st alloy produced by a method with one machining pass was used for optimization of anodic oxidation experiments.

Several experiments were carried out to investigate the effect of oxidation time on the thickness of anodic coatings (Fig. 2). The alumina layer thickness as a function of oxidation time can be described by the following function in the range between 0 and 48 h:

$$h = 0.55t + 4.6 \times 10^{-2}t^2 - 5.90 \times 10^{-4}t^3, \quad (1)$$

where $t$ is time in hours, $h$ is the layer thickness in microns. The plot of layer thickness versus oxidation time is a typical *S*-curve (Fig. 2). In the beginning of the process, the oxide layer thickness is proportional to the oxidation time. After 5 h the oxidation rate starts increasing. This corresponds to the beginning of the horizontal part of the voltage curve (Fig. 3a). Then, the oxidation rate decreases due to a decrease of the anodization current efficiency with respect to oxide formation. As a result, linear characteristics between layer thickness and oxidation time are again observed in the range between 23 and 30 h with a slope of 1.75 μm/h. At this stage, the oxidation rate more than three times exceeds its initial value. After 30 h, the rate of oxide formation monotonously decreases due to the increasing resistance of a growing alumina layer and as a result decreasing current efficiency with respect to oxide formation. This effect is discussed below.

The schematic view of a cross section of a microstructured plate before and after oxidation is shown in Fig. 4a and b, respectively, where Ox represents the thickness of oxide layer, $H$ represents the initial thickness of the aluminum plate, $M$ represents the thickness of the metal remaining beneath the oxide layer, and $R$ represents the radius of the microchannel. A typical image of the microstructured plate after oxidation is shown in Fig. 4c. If a high anodization current efficiency with respect to oxide formation current is achieved, the ratio $E$ calculated according to Eq. (2) is greater than unity, due to the lower overall density of the porous oxide film compared to the aluminum substrate [19].

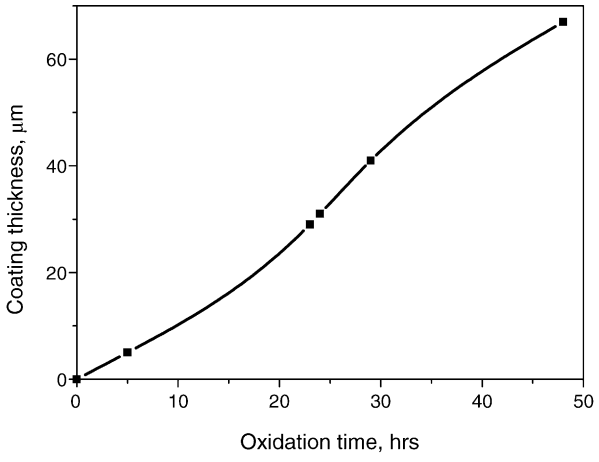


Fig. 2. The thickness of the alumina layer as a function of oxidation time on Al51st. A 0.4 M aqueous solution of oxalic acid was used as electrolyte. Anodic current density: 5 mA/cm$^2$. Temperature 1.0 ± 0.1 °C. Voltage curve is shown in Fig. 3a.

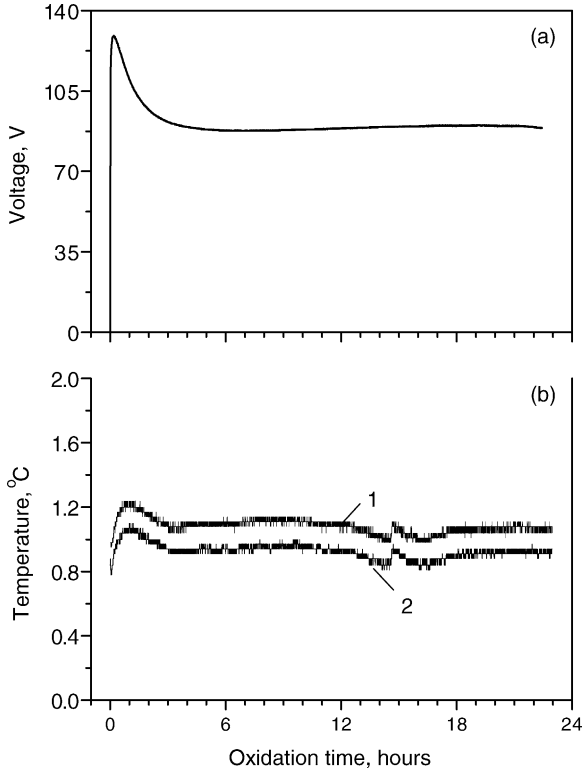


Fig. 3. (a) Voltage and (b) temperature at the top (1) and bottom (2) parts of the electrolyte solution as a function of time. The conditions are the same as those in Fig. 2.

$$E = \frac{\mathrm{Ox}}{M(0) - M} \quad (2)$$

In Eq. (2), Ox is the thickness of oxide layer, $M(0)$ is the initial thickness of the aluminum plate, $M$ is the thickness of the metal remaining beneath the oxide layer. Achieving a high anodization current efficiency is important to avoid possible significant decreases in reactor feature size due to excessive aluminum dissolution. In addition, a high anodization current efficiency promotes the conservation of aluminum metal in the "core" beneath the oxide layer, which allows for improved heat transfer throughout the reactor [19]. The results of anodic oxidation taken at different oxidation times are listed in Table 1. One may see that during a time interval between 23 and 30 h, corresponding to the second linear part of the oxidation rate plot (Fig. 2), the oxidation efficiency remains virtually

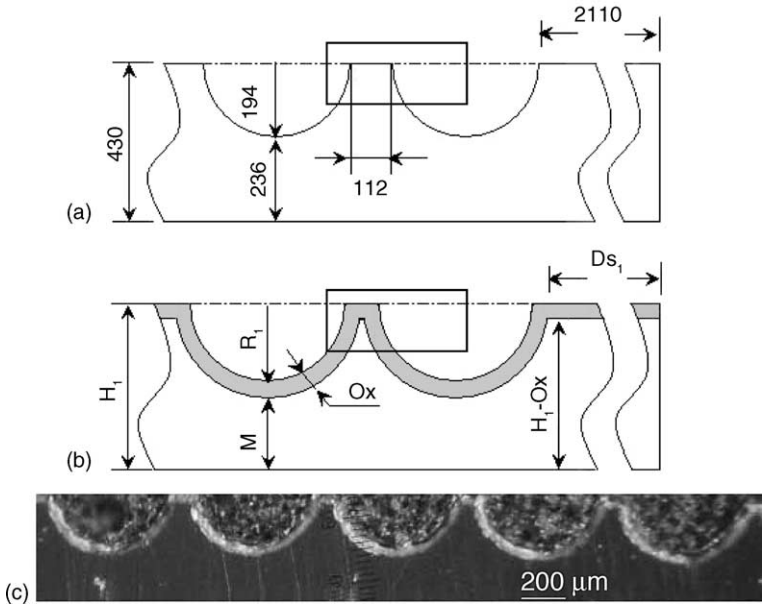


Fig. 4. Schematic view of a cross section of a microstructured plate: (a) before oxidation; (b) after oxidation; and (c) photo of a single plate after oxidation. All sizes are given in microns. Ox represents the thickness of oxide layer, $H_1$ represents the thickness of the aluminum plate, $M$ represents the thickness of the metal remaining beneath the oxide layer, $R_1$ represents the radius of the microchannel, and $Ds_1$ represents the distance between the last channel and the edge of the plate. The area inside the frames is shown in Fig. 11 under a larger magnification.

constant, but decreases considerably when the thickness of the alumina layer exceeds 30 μm.

In the course of oxidation, copper from the Al51st alloy dissolves in the electrolyte and is reduced at the platinum cathodes because its standard reduction potential $E^0_{Cu^{2+}/Cu} = 0.34$ V) is higher than that for protons (0 V). Other elements from the alloy have standard reduction potentials below 0 V, and they cannot be reduced because their concentrations in the solution are far below the concentration of protons (0.4 M). If we assume that all copper from the alloy is dissolved in the electrolyte, we can compare the mass of copper deposited at the cathodes with the mass of copper present in the dissolved volume of the alloy. The Al51st alloy has a density of 2.71 g/cm$^3$ and contains 0.1 wt.% Cu. The volume of alloy dissolved is calculated based on the data of Table 1 according to the method described in Appendix A. The decrease in the metal volume after oxidation for 23 h gives a value of 0.0396 cm$^3$ per plate. Eight oxidation runs were carried out for 23 h to provide a higher precision. The total mass of copper, which would be dissolved is

$$m_{Cu} = 8 \times 0.039\,\text{cm}^3 \times 2.71\,\text{g/cm}^3 \times 0.001 = 8.6 \times 10^{-4}\,\text{g} \quad (3)$$

The mass of copper deposited at the cathodes was $3.8 \times 10^{-3}$ g after eight oxidation runs. The concentration of Cu in the electrolyte solution of 1.1 L was below $10^{-6}$ M, so the mass of copper in the solution can be neglected in the calculations. The comparison of expected copper mass with the experimental observation clearly demonstrates that the substrate material in the vicinity of microchannels is more than four times enriched by copper after the EDM process comparing to the bulk substrate. However, copper enrichment can be considerably higher, because only the outermost 5 μm of the 29 μm layer create a large resistance to the current, and as a result a voltage maximum is observed in the beginning of the anodic oxidation (Fig. 3a). One may see from Fig. 3b that the heat is effectively removed from the vessel, so the maximum is related to a non-uniform chemical composition of the plates, but not to the differences in the electrolyte temperature.

The metal dissolution rate is higher at the beginning of the oxidation, as one can see from a lower value of the anodization current efficiency after 5 h (Table 1). This can also be explained by a higher concentration of copper and

Table 1
Geometry changes of A151st plates after anodic oxidation at different time intervals and corresponding oxidation efficiency

| Oxidation time (h) | $L$ (μm) | $R$ (μm) | $M$ (μm) | $H$ (μm) | $E$ |
|---|---|---|---|---|---|
| 0 | – | 194 | 236 | 430 | – |
| 5 | 5 | 199 | 231 | 435 | 1.00 |
| 23 | 29 | 208 | 211 | 448 | 1.16 |
| 24 | 31 | 207 | 209 | 447 | 1.15 |
| 29 | 41 | 204 | 200 | 445 | 1.14 |
| 48 | 67 | 200 | 171 | 438 | 1.03 |

$E$ is the oxidation efficiency, $E = \text{Ox}/(M\ (0) - M)$, $M(0)$ is the initial thickness of the aluminum plate, Ox is the thickness of oxide layer, $R$ is the radius of the microchannel, $M$ is the thickness of the metal remaining beneath the oxide layer, $H$ is the overall thickness of the aluminum plate. Oxidation temperature: 1 °C, oxalic acid concentration: 0.4 M, anodic current density: 5 mA/cm$^2$.

probably other alloying elements in the outermost metal layer. These elements cannot be incorporated into the oxide layer, therefore they are dissolved in the solution, decreasing the overall efficiency of the process. It has to be noted that an intensive gas evolution was observed in the first few hours of the process demonstrating that a part of the current is consumed in the side processes (4) and (5), decreasing overall efficiency:

$$C_2O_4^{2-} \rightarrow 2\,CO_2 + 2e \quad (4)$$

$$H_2O \rightarrow O_2 + 2H^+ + 2e \quad (5)$$

There are three factors, which are responsible for high copper content in the outermost layer. First, copper from the electrode, might be deposited on the microchannels in the EDM process. Secondly, high energy applied during the first machining pass can create a local temperature hot spot at the outer surface of the alloy. This allows migration of the alloying elements from the bulk to the surface. Finally, a gray residue of ca. 1 μm in thickness, present on the surface of the microchannels after a sodium hydroxide-based etch, seems also to create a resistance to the oxidation process. This residue consists of particles of oxide, intermetallics, silicon and copper, which are insoluble in the alkaline solution, but still are quite strongly fixed to the surface.

Under appropriate conditions on properly prepared substrates, an array of nanometer-scale pores can be formed. An average roughness of the alumina surface was 2 μm. SEM at larger magnification revealed the presence of pores with a diameter close to 40 nm (Fig. 5). This data agrees with the observations of others who have attempted to tune pore diameter by adjusting the anodization current density [3,17,18]. Pore size distribution data (not shown) confirmed the presence of the pores with diameter ca. 40 nm. X-ray diffraction analysis of anodized plates (not shown) showed intense peaks of aluminum substrate at 38.5 and 44.8° 2$\theta$. (International Center for Diffraction Data, ICDD 04-0787). No bands related to alumina were found.

### 3.3. Development of procedure for catalyst deposition

The typical conditions of the catalyst preparation and results of the analysis of Cu–Cr-oxide catalysts are listed in Table 2. The formed copper chromite with spinel structure is dissolved in γ-alumina with a similar structure during calcination of reference samples P(26)-400, P(26)-500, and P(26)-700. In the whole temperature range studied, five peaks are observed in the XRD spectra of reference samples at 29.60, 31.10, 35.19, 37.72, and 42.35° 2$\theta$ (not shown). This confirms the formation of a spinel structure (Cu, Cr)$[Cr,Al]_2O_4$ (ICDD 34-0424) with particle size less than 5 nm.

The concentration of copper dichromate solution, duration of impregnation, and number of impregnation cycles were varied and different aftertreatments, viz. washing or removal of impregnating solution by vacuum cleaning or by wiping, were applied in the experiments with A-plates. Washing removed most of Cu and Cr from the support. The mode of removal of excess impregnating solution (wiping or vacuum cleaning) has no influence on the catalyst loadings, but when this operation was omitted (sample A(5.3)-I), the active metals loading in the coatings was higher. Duration of impregnation has no effect on the chemical composition, due to weak chemisorption of copper and chromium from the solution. The absence of chemisorption was proved in an experiment with sample A(0.1)-I. An impregnation time of 17 h, followed by a 5 min washing step, led to trace amounts of copper and chromium

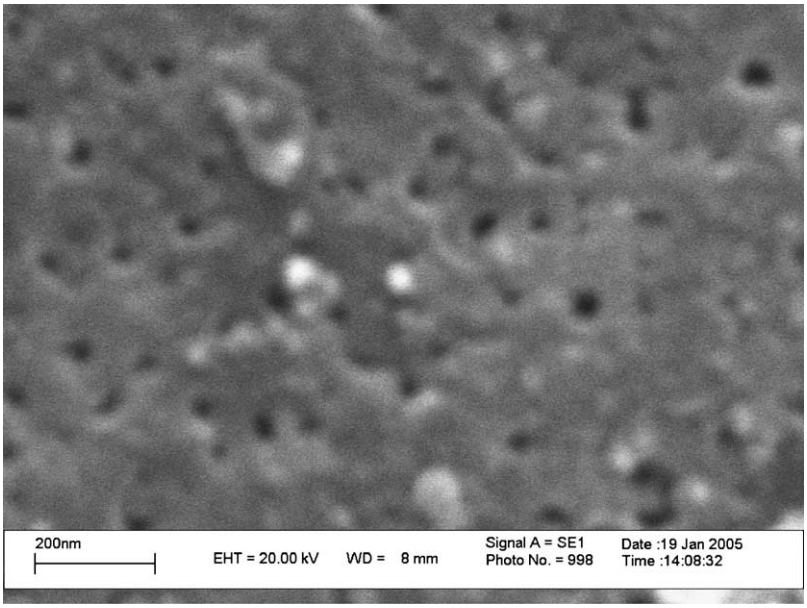


Fig. 5. SEM image of alumina coating on A-plate.

Table 2
Condition of preparation and results of chemical analysis for the supported Cu–Cr-oxide catalysts.

| Sample | Concentration of $CuCr_2O_7$ solution (mg/ml) | Impregnation time (h) | After-treatments | | Loading[a] wt. %, to mass of $Al_2O_3$ | | $CuCr_2O_4$ loading[b] wt.% | Color |
|---|---|---|---|---|---|---|---|---|
| | | | Washing with water[c] | Wiping off the residues of solution | Cu | Cr | | |
| P(26)-500 | 500 | 0.25 | – | n/a | 7.9 ± 0.3 | 11.2 ± 0.3 | 26 | Black |
| P(26)-700 | 500 | 0.25 | – | n/a | 7.9 ± 0.3 | 11.2 ± 0.3 | 26 | Black |
| A(0.1)-I | 250 | 17 | + | + | <0.03 | <0.05 | <0.1 | White |
| A(0.4)-I | 250 | 0.25 | Rinsing | + | 0.08 ± 0.05 | 0.21 ± 0.05 | 0.4 | Yellow |
| A(2.6)-I | 250 | 0.25 | – | + | 0.8 ± 0.2 | 1.1 ± 0.2 | 2.6 | Yellow |
| A(3.7)-I | 500 | 0.25 | – | + | 1.1+0.2 | 1.6 ± 0.2 | 3.7 | Black |
| A(5.3)-I | 500 | 1.0 | – | – | 1.6 ± 0.2 | 2.1 ± 0.2 | 5.3 | Black |
| A(3.5)-II | 250 | 0.25[d] | – | + | 0.8 ± 0.2 | 1.9 ± 0.2 | 3.5 | Yellow |
| M(3.7)-I | 250 | 0.25 | – | + | 1.2 ± 0.2 | 1.4 ± 0.2 | 3.7 | Gray |
| M(5.3)-II | 250 | 0.25[d] | – | + | 1.6 ± 0.2 | 2.1 ± 0.2 | 5.3 | Gray |

[a] The mass of the alumina layer is 3.8 wt.% of the mass of A samples. The mass of the alumina layer is 9.3 wt.% of the mass of M samples for the coating thickness of 29 μm. In the latter case, volume of a single plate after oxidation, obtained according to the procedure described in Appendix A, is 0.312 cm. Volume of the alumina layer is 0.043 $cm^3$. Density of the Al51st is 2.7 $g/cm^3$. Apparent density of the alumina layer is 2.0 $g/cm^3$.
[b] Calculated with apparent density of the alumina layer of 2.0 $g/cm^3$.
[c] The sample was kept in water for 1 h.
[d] The sample was dried and calcined after first impregnation.

in the coatings. Therefore, the duration of impregnation was fixed at 0.25 h in further experiments. On the contrary, the concentration of the impregnating solution has a large influence on the chemical composition. The coatings A(0.4)-I, A(2.6)-I prepared with a diluted solution were yellow, while coating A(3.7)-I, prepared from a concentrated solution, was black. The $CuCr_2O_4$ loading was higher in the latter case. Nearly the same loading was achieved after two consecutive impregnations with the diluted solution in sample A(3.5)-II. The color of the plate remains yellow in this case. Thus, the samples with the loadings of Cu up to 1.6 wt.% and Cr up to 2.1 wt.%, based on an apparent density of alumina of 2.0 $g/cm^3$ (see Section 2.2), were obtained by changing the impregnation conditions.

Element distribution in the coatings was studied by X-ray microanalysis. Fig. 6a and b show similar behavior of the lines of different elements both along the plate and at its cross section. In Fig. 6a, the intensity of Cu Kα follows that of Cr Kα and, in most locations, that of Al Kα indicating interaction of Cr and Cu with each other and with alumina. In Fig. 6b, the maxima of Cu Kα and Cr Kα at the both sides of the plate correspond to the position of alumina layers, while an Al Kα plateau corresponds to a metal layer.

Oxidation states of Cu and Cr were studied by diffuse reflectance spectra (Fig. 7a). DRS of pelletted reference catalysts P(26)-500 and P(26)-700 were also recorded for comparison (Fig. 7b). The spectra of black samples A(3.7)-I and A(5.3)-I (the latter is not shown) have low frequency bands revealed as shoulders at ca 12,500 $cm^{-1}$ corresponding to d–d transitions in $Cu^{2+}$ ion [20], and two bands at higher frequencies of 16,000 and 19,500 $cm^{-1}$ attributed to d-d transitions in $Cr^{3+}$ [20–22], in agreement with DRS of

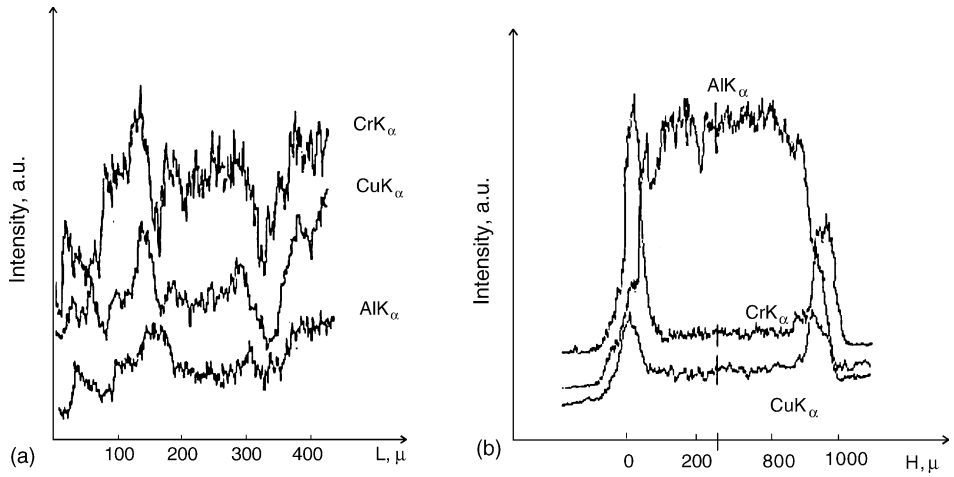


Fig. 6. X-ray microprobe analysis. Intensity of Kα Cr, Kα Cu and Kα Al lines for the sample A(3.5)-II: (a) along the plate and (b) across the plate.

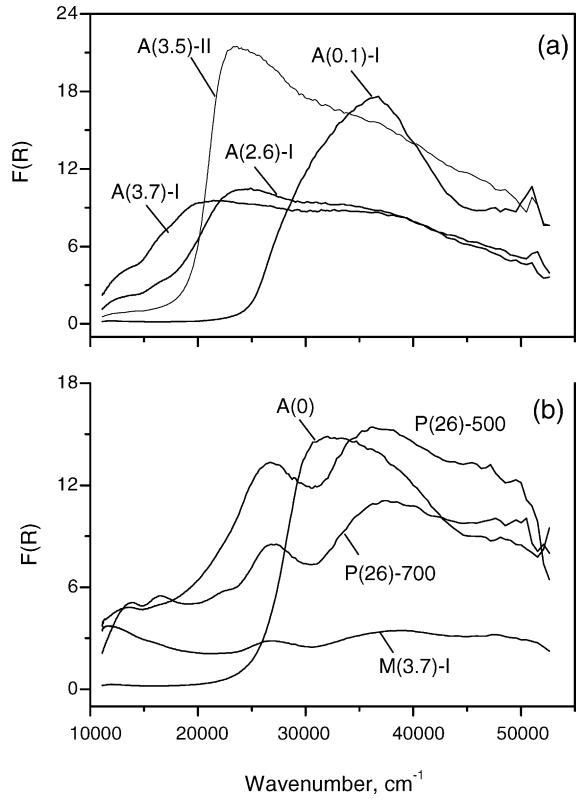


Fig. 7. (a) Diffuse reflectance spectra of catalysts supported on A-plates and (b) diffuse reflectance spectra of samples M(3.7)-I; reference samples P(26)-500, P(26)-700 Sample A(0) represents the blank experiment with a plate without active metals.

the reference samples. Spectrum of A(0.1)-I is close to that of the alumina support, due to a low $CuCr_2O_4$ loading. The spectra of samples A(2.6)-I and A(3.5)-II reveal the presence of an intense wide band near 25,000 $cm^{-1}$, which may be formed by superposition of two bands at 23,500 and 27,000 $cm^{-1}$. The position of these bands and their higher intensity with respect to lower energy bands allow the assumption that they are due to charge transfer (CT) transitions in Cr in higher oxidation states: Cr (VI) in $CrO_4^{2-}$ or $CrO_3^{-}$ type compounds [21,22]. This band is very strong, and it is characteristic of fresh catalysts calcined in air. Such catalysts usually contain an admixture of Cr(VI) [21,22], which is responsible for their high initial catalytic activity. Indeed, the intensity of the band at 26,800 $cm^{-1}$ decreases in DRS of P(26)-700 due to partial reduction of Cr(VI) to Cr(III) at high temperature revealing more clearly the bands at 16,500 and 22,500 $cm^{-1}$.

XPS data listed in Table 3, show that the main signal of copper in all Cu–Cr oxide catalysts studied is $Cu2p_{3/2}$ with almost constant BE = 932.9–933.1 eV. This peak may be assigned to $Cu^{2+}$ ions in the solid solution of $CuCr_2O_4$ [23]. Line deconvolution shows that there are also noticeable admixtures of surface copper carbonate, characterized by the BE ca. 935 eV. This is also confirmed by the BE values of C1s signal for $CO_3^{2-}$ at 290 eV. Some minor amounts of $Cu^{+}$ ions with BE ca. 932 eV are also present in the samples. The

Table 3
Results of XPS study of samples of Cu–Cr oxide catalysts on flat aluminum plates

| Sample | Binding energy (eV) | | | | | |
|---|---|---|---|---|---|---|
| | Al2s | O1s | C1s | C1s($CO_3$) | $Cr2p_{3/2}$ | $Cu2p_{3/2}$ |
| A(5.3)-I | 119.0 | 531.0 | 284.8 | 289.8 | 576.7 | 932.9<br>935.0 |
| A(0.4)-I | 119.2 | 531.2 | 284.8 | 290.0 | 577.3 | 933.1 |
| A(3.5)-II | 118.9 | 531.0 | 284.8 | 289.7 | 577.0 | 932.6<br>934.9 |

predominance of $Cu^{2+}$ is supported by the presence of $Cu^{2+}$ ''shake-up'' satellites having maxima in the BE range 933–934 eV for all samples [24,25].

It can be seen, that chromium is present mainly as $Cr^{3+}$ ions, characterized by $Cr2p_{3/2}$ BE values in the vicinity of 577 eV, which, similarly to $Cu^{2+}$ above, may be assigned to $CuCr_2O_4$ [23,24,26]. Line deconvolution and comparison with the reference spectra of $Cr_2O_3$ obtained in the same spectrometer show that minor amounts of chromium in higher oxidation states (up to +6) may be present in the catalysts. Their overall contribution is lowest for the black sample A(5.3)-I, and higher for yellow samples A(0.4)-I and A(3.5)-II in agreement with the conclusions of the DRS studies of the catalysts.

Catalytic activity of the samples in complete oxidation of butane is presented in Fig. 8. Obviously, sample A(0.4)-I with the lowest $CuCr_2O_4$ loading has the lowest butane conversion. Increasing the $CuCr_2O_4$ loading gives a rise in catalytic activity. However, despite the highest loading of an active component, sample A(5.3)-I has still low activity. This seems to be due to an omitted after-treatment step in which the residues of the impregnating solution were not removed before calcination. These residues could partly block the alumina pores leading to a decrease in activity. It is interesting to note that A(3.5)-II has twice the activity of A(3.7)-I which contains the similar amount of active component. The reason may be due to the presence of chromium in higher oxidation states as shown by DRS and XPS studies. Actually, the activity tests for 40 h showed that the activity of A(3.5)-II is not stable: the butane conversion was lower in the whole range of temperatures studied for the used A(3.5)-II sample. The intensity of the band assigned to Cr in high oxidation states was also decreased in the used A(3.5)-II sample.

### *3.4. Preparation and characterization of copper chromite catalysts on the microstructured plates*

The procedure developed on flat alumina substrate was applied to impregnate the microstructured plates. A diluted copper dichromate solution with a concentration of 250 mg/ml was used for impregnation. Impregnation time was fixed at 0.25 h, calcination for 4 h at 450 °C (see Table 2). The effect of the number of impregnation cycles (1 or 2) was studied.

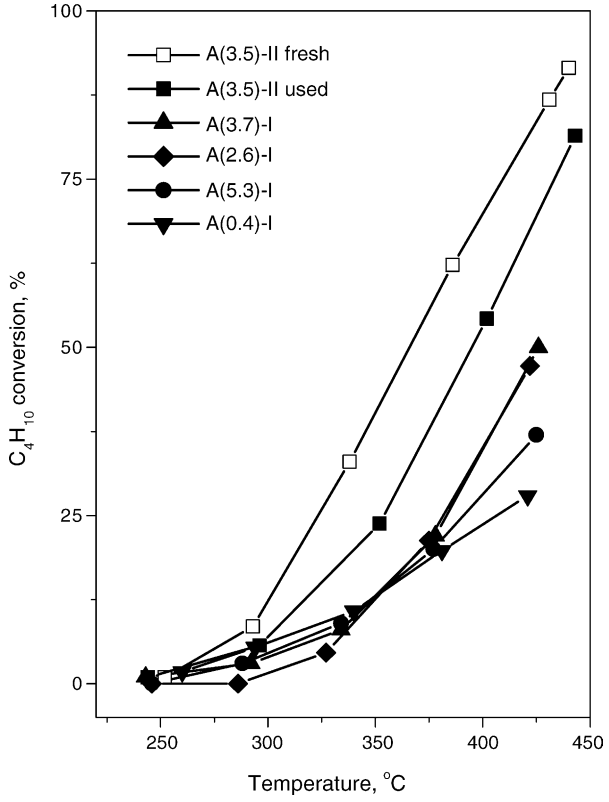


Fig. 8. Butane conversion as a function of temperature on A-plate supported catalysts. Reaction mixture: 0.2% butane in air. Flow velocity is 60 $cm^3$/min (STP); GHSV = 120,000 $h^{-1}$.

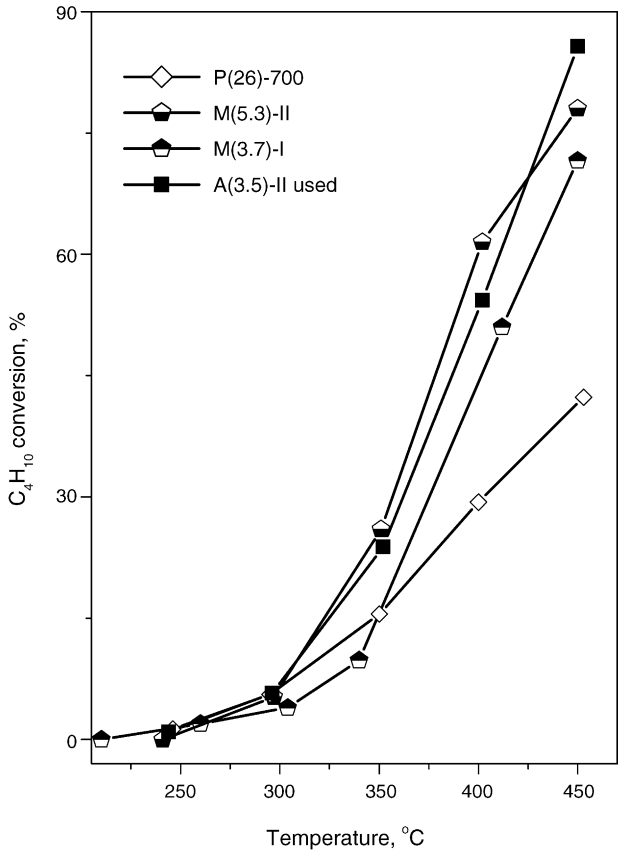


Fig. 9. Butane conversion as a function of temperature on M-plate supported catalysts. Samples A(3.5)-II(used) and P(26)-700 are given for comparison. Reaction conditions are the same as those in Fig. 8.

In contrast to the catalysts supported on A-plates, both samples supported on M-plates had a grey color. SEM images of M-plate supported catalysts revealed that the pores were not blocked after calcination, demonstrating applicability of the developed technique for preparation Cu–Cr oxide catalysts. X-ray diffraction study (not shown) of the M-plate supported catalysts showed two intense peaks of aluminum substrate (occurring at 38.5 and 44.7° 2$\theta$, ICDD 04-0787) and four peaks occurring at 24.51, 33.63, 36.23, and 41.52° 2$\theta$, which can be assigned to the $\alpha$-$Cr_2O_3$ phase (ICDD 38-1479) present in trace amounts. A weak broad band was observed in the range of 28–34° 2$\theta$. This band may be assigned to microcrystalline or X-ray amorphous alumina.

In contrast to sample A(2.6)-I, a very weak band at ca. −25,000 $cm^{-1}$ was observed in the DRS spectrum of sample M(3.7)-I prepared under similar conditions (see Fig. 7). The intensity of this band demonstrates the decrease of the Cr content, present in high oxidation states in catalysts prepared on M-plates. This effect can be explained by the differences in structural features and composition of anodic alumina produced on A- and M-plates, due to different distribution of alloying elements in M-plates after the EDM process. The alumina on A-plates seems to stabilize admixtures of Cr in high oxidation states while alumina on M-plates stabilizes $Cr^{3+}$ ions.

Fig. 9 demonstrates that Cu–Cr oxide catalysts prepared on M-plates have activities close to that of used A(3.5)-II sample. The activity of M-samples was higher than that of the reference pelletized catalyst P(26)-700. To quantitatively evaluate the advantages of the catalytic coatings, it is necessary to evaluate the influence of internal diffusion on the reaction rate. The Weisz modulus allows for the estimation of intra-particle diffusion limitations:

$$\psi = \eta\varphi^2, \tag{6}$$

where $\eta$ is the effectiveness factor, $\varphi$ is the Thiele modulus.

For a spherical particle:

$$\varphi_p = \frac{r_p}{3}\sqrt{\frac{R_{rxn}}{D_e C_s}} \tag{7}$$

where $R_{rxn}$ is the effective reaction rate, mol $m^{-3}$ $s^{-1}$; $D_e$ is the effective diffusivity of limiting reactant (butane) in the catalyst pores, $m^2$ $s^{-1}$; $r_p$ is the catalyst particle radius, $m$; and $C_s$ is the concentration of limiting reactant at the catalyst surface, mol $m^{-3}$.

For the coatings

$$\varphi_c = \mathrm{Ox}\sqrt{\frac{R_{rxn}}{D_e C_s}} \tag{8}$$

If we assume $\eta \cong 1$, the Weisz modulus equations for a spherical particle ($\psi_p$) and the coating ($\psi_c$) can be written as follows:

$$\psi_p = \frac{R_{rxn} r_p^2}{9 D_e C_s} \quad (9)$$

$$\psi_c = \frac{R_{rxn} Ox^2}{D_e C_s} \quad (10)$$

The Weisz modulus below 0.1 ($\psi < 0.1$) indicates that the catalyst layer (particle) is small enough to prevent concentration gradients from forming internally. The Weisz modulus for P(26)-700 is calculated based on the reaction rate value obtained in [27]. In an excess of oxygen, the reaction has the first order with respect to butane and the zero order with respect to oxygen. The reaction rate at 300 °C is equal to 0.115 mol $m^{-3}$ $s^{-1}$ and the activation energy is 75 kJ/mol. The effective diffusivity of butane at 300 and 400 °C is $4.8 \times 10^{-6}$ and $6.1 \times 10^{-6}$ $m^2$ $s^{-1}$, respectively. These values are obtained using a bed void fraction of 0.5, and particle tortuosity of 3. The reaction rate on the M(5.3)-II coating is calculated using the differential reactor approximation (at conversions below 10%). The reaction rate at 300 °C is equal to 0.170 mol $m^{-3}$ $s^{-1}$, which is 1.5 times higher than that of P(26)-700. Similar value is obtained for used A(3.5)-II. The activation energy is $81 \pm 2$ kJ/mol, which is close to the value obtained on P(26)-700. A void fraction of 0.2 (based on the BET data), and layer tortuosity of 1.0 (due to the cylindrical geometry of the pores) were used to calculate the effective diffusivity of butane in the coatings. The Weisz modulus values for P(26)-700 and M(5.3)-II are listed in Table 4. Internal diffusion limitations are observed for P(26)-700 above 370 °C. There is an increasing difference between the catalytic activity of coatings and P(26)-700 in the high temperature range due to the presence of internal diffusion limitations in the latter case. The effectiveness factor for P(26)-700 at 400 °C is ca. 0.8, while the reaction on the coatings is under kinetic control in the whole temperature range studied. This clearly demonstrates the advantages of using catalytic coatings rather than pelletized catalysts.

The Cu–Cr oxide catalysts prepared on M-plates have also a high stability. Fig. 10 demonstrates the activity in butane oxidation for sample M(5.3)-II at 350 °C. One can see that activity stays at the same level for time on stream for at least 40 h.

Table 4
Comparison of the reaction rate and the Weisz modulus for P(26)-700 and M(5.3)-II

| Temperature (°C) | P(26)-700 | | M(5.3)-II | |
|---|---|---|---|---|
| | $R_{rxn}$ (mol/$m^3$ s) | $\psi_p$ | $R_{rxn}$ (mol/$m^3$ s) | $\psi_c$ |
| 300 | 0.115 | 0.029 | 0.170 | $6.5 \times 10^{-4}$ |
| 400 | 1.18 | 0.322 | 1.60 | 0.0083 |

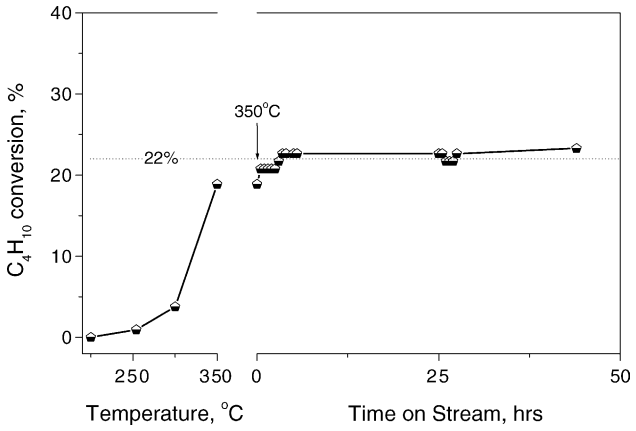


Fig. 10. Butane conversion vs. time on stream for catalyst M (5.3)-II. Temperature: 350 °C. The other conditions are the same as those in Fig. 8.

## 4. Conclusions

The effect of different electro discharge machining techniques on the geometrical parameters of the micro-structured plates produced in two different aluminum alloys has been studied. Al99.5 material can be applied as a substrate material for machining microchannels with a length to diameter ratio below 50. An alloy with relatively high content of alloying elements (Al51st) should be used in case of microchannels with a high length to diameter ratio of 100. The method with two machining passes has to be applied to decrease the surface roughness of microchannels produced in Al51st to ca. 2.0 μm. A procedure of anodic oxidation of the Al51st alloy has been optimized to produce an oxide layer of 30 μm thickness in a 0.4 M oxalic acid solution under current control conditions. The electrolysis time was optimized to get a maximum anodization current efficiency with respect to oxide formation. The temperature of electrolyte was fixed at 1 °C to avoid extensive dissolution of substrate material. A novel design of the electrolysis cell was proposed and validated to provide a simultaneous oxidation of 12 identical substrates. In this design, the maximum temperature non-uniformity does not exceed 0.2 °C, providing a uniform thickness and uniform pore size distribution. Alumina coatings with an average pore diameter of 40 nm are produced.

The synthesis of copper chromite coatings was performed by impregnation of the alumina coating with an aqueous solution of copper dichromate followed by drying and calcination. The preparation method used provides a uniform metal distribution along the plates. DRS and XPS studies revealed the predominant formation of $Cu^{2+}$ and $Cr^{3+}$ ions with binding energies close to those found in $CuCr_2O_4$. An admixture of chromium in higher oxidation states may be responsible for a higher initial activity of the catalysts in the total oxidation of n-butane. In the course of the reaction, the reduction of high-valent chromium species takes place, which reduces the catalytic activity of these samples by 20–25%. The coatings with only trace amounts

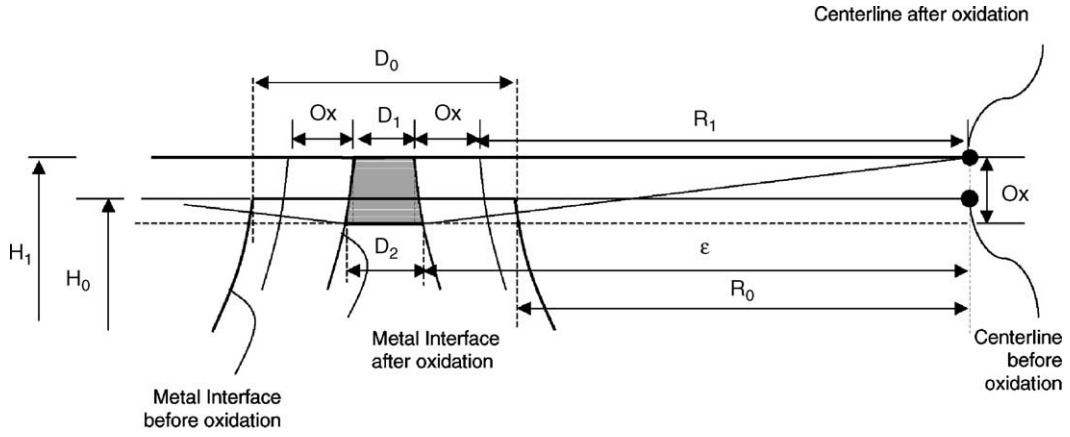


Fig. 11. Schematic view of a part of M-plate with two adjacent microchannels and a metal space in between. The metal–gas interface before oxidation and metal–oxide interface after oxidation are drawn in bold line. The situation before and after oxidation is sketched individually in a height-shifted manner in Fig. 4a and b. The parameter names are the same as those given in Fig. 4. Subindex "0" denotes the initial values of the parameters. Subindex "1" denotes those after oxidation.

of chromium in higher oxidation states demonstrated high and stable activity from the beginning. Even at much lower loadings of active metals, the catalytic activity of the prepared coatings, related to the volume of the alumina layer, is superior to that of pelletized catalysts. Microreactors made according to these procedures can be used for a variety of small-scale total oxidation processes involving combustion of toxic and hazardous chemicals.

## Acknowledgements

The financial support by the Netherlands Organization for Scientific Research (NWO) and Russian Foundation for Basic Research (RFBR), project 047.15.007 is gratefully acknowledged. We are grateful for assistance in catalyst characterization to Dr. V.A. Ushakov (XRD), Dr. I.A. Ovsyannikova (X-ray microprobe), Dr. A.I. Boronin and Dr. S.V. Koshcheev (XPS), Dr. T.V. Larina (DRS), Dr. N.A. Rudina (SEM), and Mr. V.V. Kuznetsov (long-term activity tests). Special thanks to Prof. Z.R. Ismagilov for fruitful discussions.

## Appendix A. Change of metal volume after oxidation

Fig. 11 demonstrates a part of the channel with a metal part in between. The initial metal volume is

$$V_0 = \left[(N(2R_0 + D_0) - D_0 + 2Ds_0)H_0 - \frac{N\pi R_0^2}{2}\right]L \quad (11)$$

The volume after oxidation is

$$V_1 = \left[(N(2(R_1 + \mathrm{Ox}) + D_1) - D_1 + 2Ds_1)H_1 - \frac{N\pi(R_1 + \mathrm{Ox})^2}{2} - (N-1)S_1 - 2S_2\right]L \quad (12)$$

Subscript "0" denotes the initial values of the parameters. Subscript "1" denotes those after oxidation. $S_1$ is the area of the gray trapezoid (see Fig. 11),

$$S_1 = \mathrm{Ox}\frac{D_1 + D_2}{2} \quad (13)$$

where

$$D_1 = D_0 - 2\delta \quad (14)$$

$$\delta = R_1 + \mathrm{Ox} - R_0 \quad (15)$$

$$D_2 = D_1 + 2(R_1 + \mathrm{Ox} - \varepsilon) \quad (16)$$

$$\varepsilon = \sqrt{(R_1 + \mathrm{Ox})^2 - \mathrm{Ox}^2} \quad (17)$$

Inserting the expressions for $D_1$ and $D_2$ into (13), one arrives at

$$S_1 = \mathrm{Ox}(D_0 + 2R_0 - R_1 - \mathrm{Ox} - \sqrt{(R_1 + \mathrm{Ox})^2 - \mathrm{Ox}^2}) \quad (18)$$

Area $S_2$ represents the oxide layer on a flat part of M-plates (between the edge and the first channel and between the last channel and the edge). This area can be approximated by the area of the rectangle:

$$S_2 \cong \mathrm{Ox}\, Ds_1 \quad (19)$$

where

$$Ds_1 = Ds_0 - \delta \quad (20)$$

Initial values of parameters are given in Fig. 4a. Values after oxidation for 23 h are given in Table 1.

## References

[1] S. Ihm, E. Ruckenstein, Ind. Eng. Chem. Prod. Design Dev. 17 (1978) 110.

[2] G. Patermarakis, C. Pavlidou, J. Catal. 147 (1994) 140.
[3] G. Patermarakis, N. Nicolopoulos, J. Catal. 187 (1999) 311.
[4] J.C. Ganley, K.L. Riechman, E.G. Seebauer, R.I. Masel, J. Catal. 227 (2004) 26–32.
[5] A. Hitoshi, Method for processing anodic oxidation film different in thickness in front and back, Patent JP2001271199 (2001).
[6] G. Wiessmeier, D. Haönicke, J. Micromechan. Microeng. 6 (1996) 285.
[7] K. Toshihiro, K. Shinpei, Apparatus for anodic oxidation-treatment to aluminum or aluminum alloy, Patent JP2004211116 (2004).
[8] Z.R. Ismagilov, M.A. Kerzhentsev, Catal. Rev. Sci. Eng. 32 (1990) 51.
[9] H. Charcosset, P. Turlier, G. Trambouze, J. Chim. Phys. Phys. Chim. Biol. 61 (1964) 1249.
[10] L.V. Feshchenko, V.L. Vlasenko, V.L. Chernobrivets, Khim. Tekhnol. 4 (1982) 12.
[11] R.V. Chesnokova, A.M. Alekseev, A.A. Bondareva, Zh. Neorg. Khim. 12 (1976) 36.
[12] O.V.Korotkikh, Ph.D. thesis, Boreskov Institute of Catalysis, Novosibirsk, Russia, 1995.
[13] E.V. Rebrov, M.H.J.M. de Croon, J.C. Schouten, Catal. Today 69 (2001) 183.
[14] J.C. Schouten, E.V. Rebrov, M.H.J.M. de Croon, Chimia 56 (2002) 627.
[15] E.V. Rebrov, S.A. Duinkerke, M.H.J.M. de Croon, J.C. Schouten, Chem. Eng. J. 93 (2003) 201.
[16] E.V. Rebrov, M.H.J.M. de Croon, J.C. Schouten, Chem. Eng. Res. Des. 81A (2003) 744.
[17] V. Parkhutik, V. Shershulsky, J. Phys. D: Appl. Phys. 25 (1992) 1258.
[18] G. Patermarakis, K. Moussoutzanis, Corrosion Sci. 43 (2001) 1433.
[19] J.C. Ganley, K.L. Riechmann, E.G. Seebauer, R.I. Masel, J. Catal. 227 (2004) 26.
[20] G.L. Castiglioni, A. Vaccari, G. Fierro, M. Inversi, M. Lo Jacono, G. Minelli, I. Pettiti, P. Porta, M. Gazzano, Appl. Catal. A 123 (1995) 123.
[21] B.M. Weckhuysen, A.A. Verberckmoes, A.R. De Baets, R.A. Schoonheydt, J. Catal. 166 (1997) 160.
[22] D.A. Arendarskii, E.A. Paukshtis, Z.R. Ismagilov, E.N. Yurchenko, React. Kinet. Catal. Lett. 28 (1985) 195.
[23] NIST XPS v. Database 3.4, www.nist.gov/srd/online.htm.
[24] D.A. Arendarskii, A.V. Pashis, A. Shepelin, Z.R. Ismagilov, React. Kinet. Catal. Lett. 28 (1985) 211.
[25] D.C. Frost, A. Ishitam, C.A. McDowekk, Mol. Phys. 24 (1972) 861.
[26] C.A. Best, R.G. Squitres, R.A. Walton, J. Catal. 57 (1977) 292.
[27] Z.R. Ismagilov, O.Yu. Podyacheva, M.A. Kerzhentsev, V.N. Bibin, A. Ermakova, G.K. Chermashentseva, Kinetika i Kataliz 29 (1988) 254 (in Russian).